Coordinated Control of Three Single–Phase BESS Inverters Using Local Measurements to Mitigate Voltage Unbalance

Ioannis Mexis, *Student Member, IEEE*, Grazia Todeschini, *Senior Member, IEEE*, and Zhongfu Zhou

***Abstract*—This paper proposes a control algorithm for single-phase battery inverters to provide voltage unbalance compensation in distribution networks with high penetration of photovoltaic panels and electric vehicles. A typical distribution system is studied to quantify the impact of single-phase loads and generating units on voltage unbalance levels, and identify the conditions that lead to the highest voltage unbalance. Voltage unbalance compensation is then performed by regulating active and reactive power exchange between three single-phase battery energy storage units and the power grid. The proposed control strategy consists of an upper level control system to coordinate the three units by sending active and reactive power reference signals, and a BESS control system to regulate active and reactive power exchange between each single-phase inverter and the grid. Simulation results show that the effectiveness of this approach depends on the location where the energy storage units are installed. The positive impact of the proposed methodology on balancing the power flow and reducing the transformer zero-sequence current is also demonstrated. Finally, Hardware-In-The-Loop (HIL) experiments are carried out to provide validation of the control algorithm in real-time.**

***Index Terms*—Ancillary services, battery energy storage systems, voltage unbalance compensation, voltage unbalance factor, single–phase inverter.**

I. Introduction

In the last decade, an increasing number of distributed energy resources (DERs), such as photovoltaic (PV) distributed generation and plug-in electric vehicles (PEVs), has been deployed in distribution networks worldwide [1]. This trend is expected to continue and to further accelerate in order to meet Net Zero targets. Since a large portion of these devices is single-phase connected, and given the cumulative large power rating and their variable output, voltage unbalance levels are expected to increase across distribution feeders and at the substations. This in turn will degrade the grid power quality by causing higher network losses, reduction of the effective utilization of the distribution line capacity and transformer overheating due to zero-sequence fundamental current in the neutral conductor [2], [3].

As a result of the above challenges, to maintain a balanced system operation, distribution network operators (DNOs) are exploring new approaches to improve voltage profiles and reduce unbalance levels. Series and parallel active power filters have been proposed for voltage unbalance compensation by injecting negative-sequence voltage and current, respectively [4]. Furthermore, voltage unbalance can be reduced by controlling unified power quality conditioners to inject both negative-sequence voltage and current or by static synchronous compensators controlled to inject positive- and negative-sequence reactive power [5]. However, the aforementioned solutions incur in high costs for DNOs [6].

Alternatively, power converters used for distributed generation (DG) may provide voltage unbalance compensation as an ancillary service by regulating their reactive power output [1]. However, the effectiveness of this method is limited to low voltage (LV) networks with high R/X values. In [6], three-phase inverters for wind and solar generation are controlled to compensate voltage unbalance at the PCC by injecting negative-sequence active and reactive power, while in [7] the negative- and zero-sequence grid current components are compensated by single-phase DG inverters. A supervisory controller manages the units by calculating the reactive power references for each inverter in real time [8]. The control strategy presented in [9] enables the synergic action of single-phase and three-phase PV inverters for voltage unbalance mitigation, with a central controller located at the PCC evaluating the required compensating active and reactive power signals to be dispatched to the inverters. More recently, decentralized and distributed control schemes based on the Steinmetz design have been proposed to control the reactive power injections of single-phase distributed PV inverters for voltage unbalance mitigation [10].

All the works cited above refer to the use of wind/solar inverters. Despite the potential benefits of using Battery Energy Storage Systems (BESSs) for voltage unbalance compensation, due to their declining prices, flexibility to control both active and reactive power (four-quadrant operation) and relatively stable DC voltage, such application is a relatively unexplored research area. Only a few literature works consider using BESSs for providing phase balancing services, and most of these research papers focus on three-phase BESSs. In [2], a control scheme is proposed for three-phase PV/BESS inverters installed across a distribution system to balance the voltage at the LV busbar; a central controller receives measurements from a smart meter installed at the MV/LV transformer and calculates the negative-sequence reference set-points sent to each inverter. A three-phase community energy storage (CES) system was proposed in [11] to alleviate the neutral current and neutral-to-ground voltage rise caused by the variable PV output and unbalanced loads in a multi-grounded three-phase

The Authors are with the Faculty of Science and Engineering, Swansea University, UK (943364, grazia.todeschini, z.zhou@swansea.ac.uk)

G. Todeschini is also with the Department of Engineering, King's College, London, UK (grazia.todeschini@kcl.ac.uk)

four-wire distribution system. The CES system was controlled to dynamically balance the power exchange with the grid utilizing the minimum amount of power.

The provision of unbalance compensation by single-phase BESS has been described only by a few authors. In [12], PEVs single-phase batteries were coordinated to inject and absorb reactive power to mitigate the current unbalance. However, since the active power exchange remains unaltered, the effectiveness of this method is limited for distribution systems with high PV and EV penetration levels. In [13], the control of a single-phase BESS connected at the same phase as a PV inverter and a load reduces the voltage unbalance and the network power losses by acting as a load or generator when the PV output is greater or lower than the load, respectively. Nevertheless, the proposed control scheme results in voltage unbalance levels above the statutory limit and increased network losses when the BESS is connected at different phase from the PV and the load. Distributed control strategies for single-phase distributed BESSs were proposed in [14] to balance the active powers at the point of common coupling (PCC) of the distribution system. In [15], the power balancing algorithm proposed in [11] was applied to single-phase battery storage devices integrated with PV systems in the distribution feeder to balance the power flows at each bus, by storing surplus energy during PV peak generation period and releasing the stored energy during the evening peak load.

This paper proposes a novel control strategy to use single-phase BESS units to compensate voltage unbalance due to the presence of single-phase loads, EVs and PVs in a distribution system. Single-phase BESS inverters are controlled to inject both active and reactive power based on local measurements, with the intent of mitigating voltage unbalance at the bus where they are connected, and consequently across the distribution system. The proposed strategy can be implemented as ancillary service, in addition to other functions such as, for example, load balancing [1]. Additionally, this strategy can be deployed to other assets including energy storage, such as EVs. This paper will focus only on voltage unbalance mitigation for stand-alone battery units, and will show that the single-phase BESS units can be connected either at the substation or at other busbars along the distribution feeder, and the BESS location results in varying degree of effectiveness of the developed control strategy.

The novelty of the proposed approach is that it is based on the coordinated operation of three independent single-phase BESS inverters. The three units receive reference active and reactive power signals from an upper level control system, while the BESS control system is responsible to regulate the current output of each inverter. This solution offers enhanced reliability and greater flexibility compared to the use of three-phase inverters, since the proposed functionality may be deployed either by the three units simultaneously or by an individual inverter, depending on factors such as the availability of each BESS or the unbalance profile of the system under consideration. As an example, for a three-phase feeder with the heavy loading in one phase, it may be unnecessary to deploy the proposed functionality in the three units at the same time. It will be shown that placement of the BESSs at the substation may lead to more balanced power flows at the distribution transformer, thereby achieving more effective utilization of the line capacity. Finally, the proposed control scheme can alleviate the neutral current.

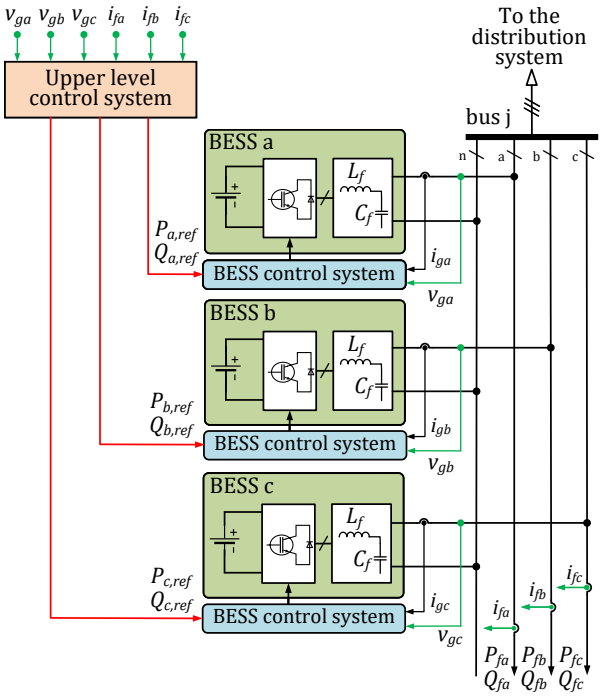

Fig. 1. Schematic of the three single-phase BESS units connected to the distribution system for providing voltage unbalance compensation.

Another novel contribution of this work is to assess the impact of increasing PV and EV penetration levels on voltage unbalance for a typical UK distribution system. To this end, realistic load, PV and EV profiles were modelled, and various scenarios were simulated by varying the number of devices connected to the distribution network. The impact of the proposed control strategy was tested via simulations initially, followed by Hardware-In-The-Loop (HIL) tests.

The paper is organized as follows. Section II introduces the proposed control strategy for voltage unbalance mitigation, and describes both the upper level control system and the BESS control system. The distribution system under consideration is presented in Section III. In Section IV, simulation results for various PV and EV penetration levels are provided, and the effectiveness of the developed control algorithm on voltage unbalance mitigation is demonstrated. Experimental validation of the BESS control is carried out in Section V. Section VI draws the concluding remarks.

II. Voltage Unbalance Compensation Strategy

Figure 1 illustrates the configuration of three single-phase BESS units connected at a generic bus (labelled 'bus j') and the control system layout. This representation means that the BESS units may be connected either at the substation busbar or at any other three-phase busbar.

The downstream single-phase loads are represented by their active and reactive power values P_{fi}, Q_{fi}, with i = a, b, c. It is worth noticing that the term 'load' is used loosely here, as both passive and active elements (such as PVs and

EVs) may be connected to the distribution feeder, and the net power may be positive or negative, and varying in time. It is assumed that the loads are non-uniformly distributed, so that the power flow in the three phases will be different thus leading to unbalanced voltages at bus j. In this work the three-phase distribution system topology is considered symmetrical and voltage unbalance is caused by unequal load distribution.

The proposed control system is composed of two distinct parts: the upper level control system and the BESS control system. The upper level control system coordinates the three units by providing active and reactive power reference to each BESS inverter, based on voltage measurements and feeder current measurements at bus j (v_{gi} and i_{fi}, with i = a, b, c). The BESS control system regulates the active and reactive power and generates the switching pulses for the inverter based on power references ($P_{i,ref}$, $Q_{i,ref}$), voltage measurements (v_{gi}) and inverter output current measurements (i_{gi}).

The aim of the proposed strategy is to control the inverters to inject negative- and zero-sequence fundamental current components to be equal in magnitude and 180^o out of phase compared to the sequence components of the feeder current. As a result, only the positive-sequence current component flows upstream bus j. The two control systems are described in details in the next subsections.

A. Upper level control system

Figure 2 presents a detailed representation of the upper level control system. Both current and voltage signals i_{fi} and v_{gi} are transformed to the phasor domain by applying the Fourier transformation, thus leading to the signals [$\boldsymbol{I_{fa}}$, $\boldsymbol{I_{fb}}$, $\boldsymbol{I_{fc}}$] and [$\boldsymbol{V_{ga}}$, $\boldsymbol{V_{gb}}$, $\boldsymbol{V_{gc}}$]. The Fortescue transformation is then applied to obtain the current symmetrical components [$\boldsymbol{I_{f1}}$, $\boldsymbol{I_{f2}}$, $\boldsymbol{I_{f0}}$]. Since the BESS inverter is expected to inject both the zero- and the negative-sequence current components of the feeder current, $\boldsymbol{I_{f2}}$ and $\boldsymbol{I_{f0}}$ are multiplied with -1, while $\boldsymbol{I_{f1}}$ is multiplied by zero. The inverse Fortesque transformation is then applied to the modified symmetrical current components to calculate the reference current phasors [$\boldsymbol{I_{a,ref}}$, $\boldsymbol{I_{b,ref}}$, $\boldsymbol{I_{c,ref}}$]. The reference current phasors are multiplied with the voltage phasors [$\boldsymbol{V_{ga}}$, $\boldsymbol{V_{gb}}$, $\boldsymbol{V_{gc}}$] to calculate the reference active and reactive power commands ($P_{i,ref}$, $Q_{i,ref}$) for each BESS inverter. Based on the proposed control strategy, the formulations of the reference powers are:

$$\boldsymbol{S_{a,ref}} = P_{a,ref} + jQ_{a,ref} = \boldsymbol{V_{ga}}(-\boldsymbol{I_{f2}^*} - \boldsymbol{I_{f0}^*}) \quad (1)$$

$$\boldsymbol{S_{b,ref}} = P_{b,ref} + jQ_{b,ref} = \boldsymbol{V_{gb}}(-\boldsymbol{\alpha^* I_{f2}^*} - \boldsymbol{I_{f0}^*}) \quad (2)$$

$$\boldsymbol{S_{c,ref}} = P_{c,ref} + jQ_{c,ref} = \boldsymbol{V_{gc}}(-\boldsymbol{\alpha^{2*} I_{f2}^*} - \boldsymbol{I_{f0}^*}) \quad (3)$$

Reference powers are used as output of the upper level control system because conservative control variables, such as active and reactive power, are more suited when applying coordinated control strategies between various network components [9], [16]. From (1)-(3), the three BESS units are controlled to supply the zero- and negative-sequence current to the load, therefore only the positive-sequence current flows through bus j. As a result of the improved current symmetry, the voltage drops across the downstream distribution system are altered, with the voltage deviations between the three phases being reduced at the remaining buses.

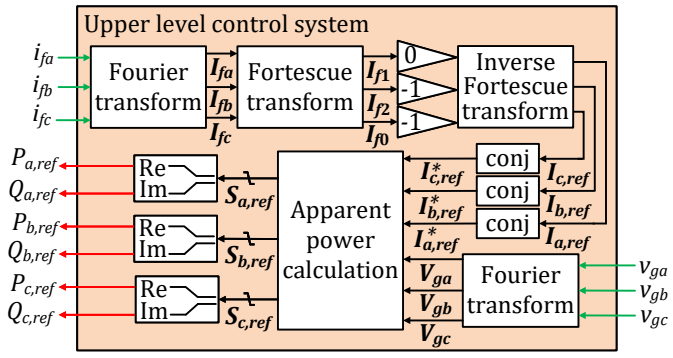

Fig. 2. Upper level control system structure.

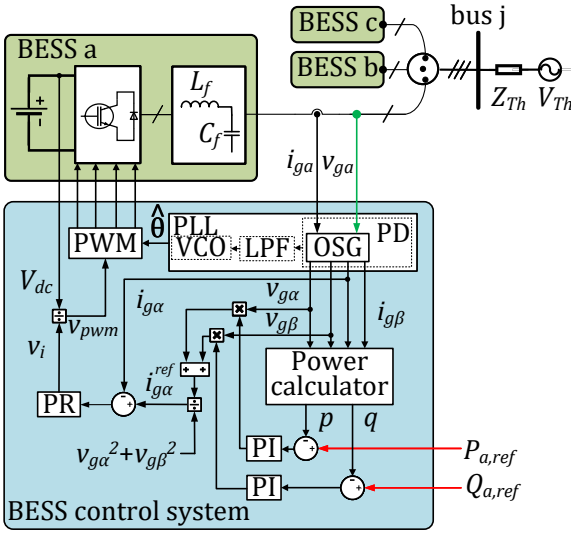

Fig. 3. Phase-a BESS inverter and BESS control system.

B. BESS control system

This section provides a high-level description of the BESS control system, while more details, including validation, can be found in [17]. The control system for phase-a BESS unit is shown in Figure 3 for simplicity. The control for phase-b and phase-c units is identical. In this figure, the three-phase network Thevenin equivalent is included. The inputs to the BESS control system are the reference powers calculated by the upper level control system ($P_{a,ref}$, $Q_{a,ref}$).

The BESS control algorithm is based on the single-phase PQ theory [17]. Since in the application under study the active and reactive power output of the inverters are controlled for voltage unbalance mitigation, the control system needs to calculate instantaneous power values.

Starting from current and voltage measurement at the BESS terminals (i_{ga} and v_{ga}), an Orthogonal Signal Generator (OSG) based on the second order generalized integrator [18]-[21] calculates the orthogonal voltage and current signals - i.e. the "α" and "β" grid voltage and current components in the $\alpha\beta$-stationary reference frame ($v_{g\alpha}$, $v_{g\beta}$, $i_{g\alpha}$, $i_{g\beta}$). From these signals, the instantaneous active and reactive power are calculated as:

$$p_a = (v_{g\alpha} i_{g\alpha} + v_{g\beta} i_{g\beta}) \times 1/2 \quad (4)$$

$$q_a = (v_{g\beta} i_{g\alpha} - v_{g\alpha} i_{g\beta}) \times 1/2 \quad (5)$$

Since the active and reactive power are dc quantities under sinusoidal and steady-state operating conditions, PI controllers are used for power regulation. The current reference in the $\alpha\beta$-stationary reference frame for the single-phase inverter is expressed as [22]:

$$\begin{bmatrix} i_{g\alpha,ref} \\ i_{g\beta,ref} \end{bmatrix} = \frac{1}{v_{g\alpha}^2 + v_{g\beta}^2} \begin{bmatrix} v_{g\alpha} & v_{g\beta} \\ v_{g\beta} & -v_{g\alpha} \end{bmatrix} \begin{bmatrix} G_p(s)(p - P_{ref}) \\ G_q(s)(q - Q_{ref}) \end{bmatrix} \quad (6)$$

where P_{ref}, Q_{ref} are the active and reactive power reference, respectively, and $G_p(s)$, $G_q(s)$ are the PI controller transfer functions. The reference current is regulated by a proportional-resonant (PR) controller: this term introduces an infinite gain to remove the steady–state error at the resonant frequency of 50 Hz [23], [24].

Notably, when the BESS cannot provide active power due to lack of charge or outages, the inverter can still inject reactive power, thus emulating the operating conditions described in [1], [12]. More formally, this condition is achieved by setting $P_{ref} = 0$ in the upper level controller.

III. Distribution System Configuration

The proposed control algorithm will be demonstrated by using a distribution system topology that is commonly adopted in the UK. The single-line diagram of the system under consideration is shown in Figure 4. The system parameters (equivalent impedance, transformer, line impedance) are summarized in Table I. These values were retrieved from [25], where typical arrangements and equipment deployed in UK distribution systems are described. The upstream voltage source is considered to be balanced, and Table II presents the main BESS parameters.

The network includes five three-phase feeders and 20 buses, labelled A_k, B_k, C_k, D_k, E_k, with $k = 1, 2, 3, 4$. The network supplies 100 single-phase loads, and in the rest of the paper they will be referred simply as 'loads' since no three-phase customers are connected. The great majority of the buses supplies three loads, except for buses B4, C4 and E4 (twelve loads each), buses B3 and C3 (six loads each), and bus E3 (ten loads). The residential demand, PV and EV profiles have been retrieved from a public database [26], [27]. This data source has been chosen since the profiles represent typical winter and summer operating conditions in the UK and allows other researchers to carry out comparative studies. Each load varies independently, and the minihmum and maximum load ratings are 1.2 and 12.3 kW, respectively. The power factor of all loads is equal to 0.98 lagging. A realistic mix of PV power sources, based on statistics presented in [26], is used: the PV nominal powers adopted in this study are rated 1, 1.5, 2.0, 2.5, 3.0, 3.5 and 4.0 kW. These ratings apply to 1, 8, 13, 14, 14, 12 and 37% of the PV panels, respectively. The EVs are assumed to have a battery rated 3 kW, 24 kWh. EVs and PVs operate at unity power factor. All profiles have a 5-min resolution.

Similarly to the loads, EVs and PVs are single-phase units - however, their connection is not indicated in the single-line diagram because various locations were considered in this work. More specifically, varying penetration levels, i.e. percentage of buses with either PVs, EVs, or both, were

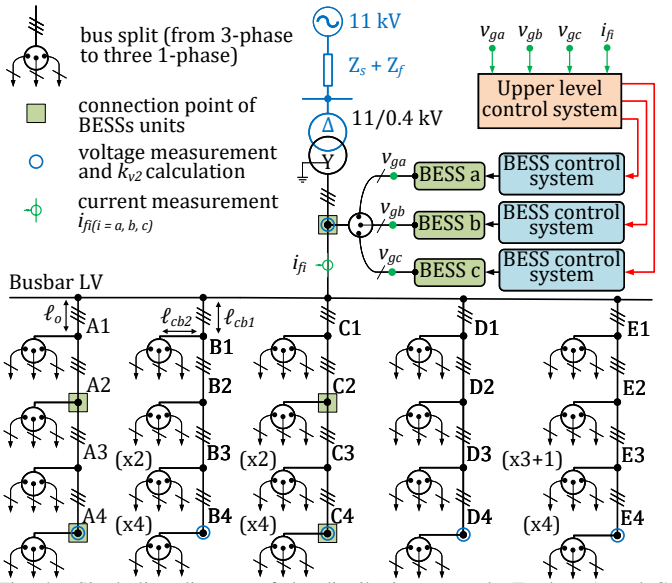

Fig. 4. Single-line diagram of the distribution network. Feeders A and C consist of overhead lines with segment length ℓ_o. Feeders B, D and E consist of cables with segment length ℓ_{cb1}, while service cables with length ℓ_{cb2} are used to connect each single-phase customer to its bus. The green squares indicate five different locations where the three BESSs are connected. The blue circles indicate the buses where voltage measurements are taken to calculate the voltage unbalance factor k_{v2}. Each arrow represents one single-phase load.

TABLE I
Upstream Grid and Distribution System Parameters.

Parameters	Values
Short–circuit power	S_k = 141 MVA, X/R = 12
Nominal voltage and frequency	V_n = 11 kV (primary); 230 kV (secondary); 50 Hz
Source impedance	$\boldsymbol{Z_s}$ = 0.069 + j0.825 Ω
11 kV feeder impedance	$\boldsymbol{Z_f}$ = 0.784 + j0.75 Ω
Transformer rated power and winding impedance	$S_{tr,n}$ = 200 kVA $\boldsymbol{z_{tr1}}$ = $\boldsymbol{z_{tr2}}$ = 0.075+j0.0225 pu
Impedance of overhead lines and cables	$\boldsymbol{Z_o}$ = 0.0716+j0.0504 Ω, ℓ_o = 200 m $\boldsymbol{Z_{cb1}}$ = 0.0287+j0.0140 Ω, ℓ_{cb1} = 200 m $\boldsymbol{Z_{cb2}}$ = 0.0236+j0.0020 Ω, ℓ_{cb2} = 30 m

TABLE II
BESS Inverter Parameters

Parameters	Values
LC filter	$R_f = 0.135$ Ω, $L_f = 3.6$ mH, $C_f = 8$ μF
Switching frequency	$f_{sw} = 10$ kHz
BESS rated power, capacity	$S_n = 9$ kVA, $E_n = 90$ kWh
BESS rated dc voltage	$V_{dc} = 500$ V
PI power controller	$k_{pp} = 0.1$, $k_{pq} = 0.1$ $k_{ip} = 10$ s^{-1}, $k_{iq} = 10$ s^{-1}
PR current controller	$k_{pi} = 20$ Ω, $k_{ii} = 150$ Ωs^{-1}
Limits for inverter power	$S_l = \pm 9$ kVA

examined with the aim to evaluate the impact of these two technologies on voltage unbalance.

The effectiveness of the proposed control methodology was evaluated for five different BESS locations (buses LV, A2, A4, C2 and C4 indicated with green squares in Figure 4). For illustrative purpose, Figure 4 shows the case when three BESS units are connected to busbar LV. In this case, the phase voltages (v_{gi} for i = a, b, c) correspond to the busbar LV voltage, and the feeder currents (i_{fi}) are measured at the secondary side of the distribution transformer. For other BESS

locations, the voltage and current measurements are taken at the terminal where the BESSs are connected. For example, when the BESSs are connected at bus A2, the upper level control system receives voltage measurements at bus A2 and feeder current measurements taken downstream of that bus. Section IV will present simulation results for the considered BESS locations.

Voltage unbalance is quantified by means of the negative–sequence voltage unbalance factor (k_{v2}). This quantity is defined in IEC 61000-2-2 as the ratio of the negative-sequence to the positive-sequence voltage fundamental component, as given below:

$$k_{v2} = \frac{|\boldsymbol{V_2}|}{|\boldsymbol{V_1}|} \tag{7}$$

The compatibility level is 2% according to [28], [29]. Here, k_{v2} is monitored at busbar LV and at the end of the feeders (buses A4-E4). These locations are marked with blue circles in Figure 4.

IV. Simulation Results

The distribution system shown in Figure 4 was modelled in MATLAB/Simulink. Two sets of simulations were carried out: the first set was intended to assess voltage unbalance levels due to increasing penetration of single-phase PVs and EVs, with no BESSs in service. These simulations will be presented in subsection A and subsection B, respectively.

The second set of simulations aimed at evaluating the effectiveness of the control strategy proposed in Section II for operating conditions corresponding to high voltage unbalance levels. To this end, three single-phase BESSs were connected at various locations, and their impact on both average and peak k_{v2} was evaluated. Subsection C will illustrate the positive impact of the proposed strategy for a scenario including both PVs and EVs.

To make the EMT simulation time manageable, the time scale was compressed such that 5 minutes in real time (the data resolution available from [26]) correspond to 0.5 seconds in the simulation.

A. Effect of varying PV penetration on voltage unbalance

Five different PV penetration levels were examined, i.e. from 20% to 100% with steps of 20%, while no EVs (and no BESSs) were connected to the network. The observation time was from 08:00 h to 16:00 h: this 8-hour period was chosen because PV power generation occurs mostly during this time frame. As a result, the impact on voltage unbalance is expected to be the maximum during this period.

Figure 5 presents the voltage unbalance factor profiles for busbar LV without and with PV for the five penetration levels. The simulation results are presented as 10-min aggregated values (based on IEC 61000-4-30 [30]) of k_{v2}. For brevity, only busbar LV profiles are plotted. Figure 5(a)-(b) show that a 20% PV penetration results in an increased value of k_{v2} during most of the simulation period compared to the case when no PVs are connected, while voltage unbalance is increasing for 40% and 60% PV penetration levels. As shown in Figure 5(c), k_{v2} starts decreasing for higher PV penetration levels.

The results for busbar LV and the end of the feeders are summarised in Table III and Table IV. Table III shows

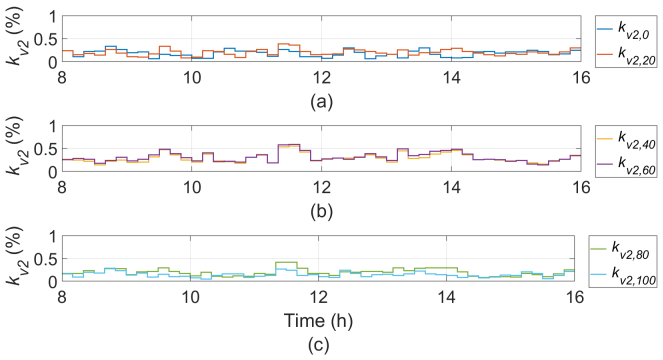

Fig. 5. Voltage unbalance factor at busbar LV without and with PVs.

TABLE III
AVERAGE VALUES OF k_{v2} FOR VARYING PV PENETRATION LEVELS.

Bus	k_{v2}(%)	PV penetration level (%)					
		0	20	40	60	80	100
LV	$k_{v2,LV}$	0.17	0.20	0.30	0.32	0.20	0.14
A4	$k_{v2,A4}$	0.36	0.58	0.68	0.68	0.49	0.30
B4	$k_{v2,B4}$	0.28	0.35	0.44	0.46	0.33	0.25
C4	$k_{v2,C4}$	0.93	0.92	1.02	1.02	0.72	0.62
D4	$k_{v2,D4}$	0.26	0.26	0.46	0.46	0.27	0.22
E4	$k_{v2,E4}$	0.30	0.31	0.38	0.44	0.51	0.27

TABLE IV
PEAK VALUES OF k_{v2} FOR VARYING PV PENETRATION LEVELS.

Bus	k_{v2}(%)	PV penetration level (%)					
		0	20	40	60	80	100
LV	$k_{v2,LV}$	0.42	0.39	0.60	0.64	0.46	0.34
A4	$k_{v2,A4}$	2.14	1.99	1.95	1.89	1.74	1.85
B4	$k_{v2,B4}$	0.96	0.96	1.05	1.00	0.86	0.81
C4	$k_{v2,C4}$	2.27	2.22	2.15	2.01	1.85	1.67
D4	$k_{v2,D4}$	0.72	0.63	0.90	0.90	0.58	0.61
E4	$k_{v2,E4}$	0.71	0.91	1.13	1.18	1.25	0.74

the average values of k_{v2} calculated at each bus and for different PV penetration levels. During the 8-hour period, k_{v2} shows an increasing trend for penetration levels up to 60%. The voltage unbalance increase is more prominent when PV penetration increases from 0% to 20% and from 20% to 40%. For penetration levels above 60%, the additional PVs have a smoothing effect, thus the value of k_{v2} decreases: this can be clearly observed by comparing the k_{v2} trend for 80% and 100% PV penetration in Figure 5. For 100% PV penetration, k_{v2} is lower then the case when no PVs are connected. Notably, these observations apply to all buses shown in Table III.

Table IV shows that peak values of k_{v2} do not follow a clear pattern, as in the case of the average values. However, at most of the buses, peak values tend to decrease for penetration levels above 80%.

B. Effect of varying EV penetration on voltage unbalance

As for the PV assessment described above, five EV penetration levels were examined, i.e. from 20% to 100% with steps of 20%, while no PVs (and no BESSs) were connected to the network. The profiles are studied from 16:00 h to 4:00 h, since most of the EVs charge within this 12-hour period.

The time-series of the voltage unbalance factor for busbar LV without and with EVs are plotted in Figure 6. Similarly to the results above, when the EV penetration level is increasing

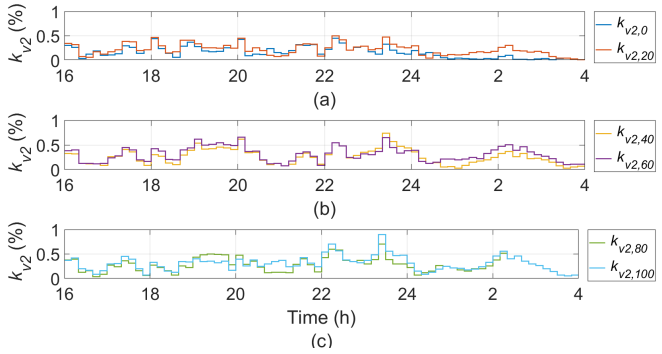

Fig. 6. Voltage unbalance factor at busbar LV without and with EVs.

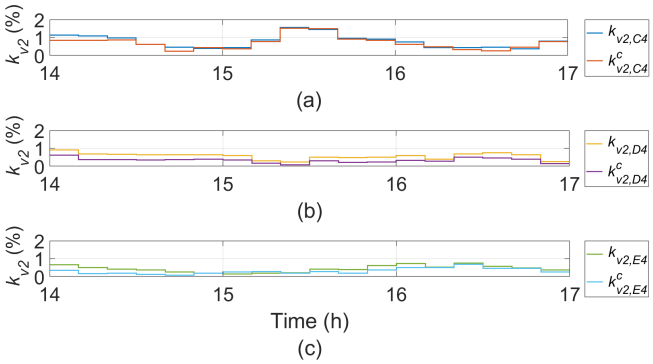

Fig. 7. k_{v2} at bus (a) C4 (b) D4 (c) E4, with and without BESS installed at busbar LV.

TABLE V
AVERAGE VALUES OF k_{v2} FOR VARYING EV PENETRATION LEVEL.

Bus	k_{v2}**(%)**	**EV penetration level (%)**					
		0	**20**	**40**	**60**	**80**	**100**
LV	$k_{v2,LV}$	0.16	0.21	0.26	0.30	0.27	0.30
A4	$k_{v2,A4}$	0.34	0.79	0.80	0.88	0.97	1.11
B4	$k_{v2,B4}$	0.28	0.43	0.46	0.52	0.51	0.63
C4	$k_{v2,C4}$	0.64	0.67	1.24	1.28	1.35	1.46
D4	$k_{v2,D4}$	0.22	0.28	0.41	0.47	0.43	0.43
E4	$k_{v2,E4}$	0.27	0.31	0.35	0.48	0.50	0.53

TABLE VI
PEAK VALUES OF k_{v2} FOR VARYING EV PENETRATION LEVEL.

Bus	k_{v2}**(%)**	**EV penetration level (%)**					
		0	**20**	**40**	**60**	**80**	**100**
LV	$k_{v2,LV}$	0.54	0.57	0.78	0.74	0.87	1.09
A4	$k_{v2,A4}$	1.43	2.24	2.3	2.33	2.33	2.98
B4	$k_{v2,B4}$	1.07	1.2	1.25	1.27	1.23	1.70
C4	$k_{v2,C4}$	3.47	3.56	4.81	4.84	7.41	7.57
D4	$k_{v2,D4}$	0.93	0.95	1.36	1.45	1.25	1.00
E4	$k_{v2,E4}$	0.94	1.06	1.06	1.24	1.37	1.71

TABLE VII
AVERAGE VALUES OF k_{v2} PER BUS FOR VARYING BESS LOCATION.

k_{v2}**(%)**	**BESS location**					
	–	**LV**	**A2**	**A4**	**C2**	**C4**
$k_{v2,LV}$	0.31	0.05	0.27	0.33	0.31	0.33
$k_{v2,A4}$	0.92	0.80	0.55	0.74	0.94	0.96
$k_{v2,B4}$	0.51	0.32	0.47	0.52	0.52	0.53
$k_{v2,C4}$	0.76	0.67	0.78	0.81	0.50	0.42
$k_{v2,D4}$	0.56	0.32	0.51	0.57	0.56	0.58
$k_{v2,E4}$	0.43	0.30	0.44	0.48	0.44	0.45

TABLE VIII
PEAK VALUES OF k_{v2} PER BUS FOR VARYING BESS LOCATION.

k_{v2}**(%)**	**BESS location**					
	–	**LV**	**A2**	**A4**	**C2**	**C4**
$k_{v2,LV}$	0.97	0.72	0.99	1.05	1.00	1.06
$k_{v2,A4}$	1.67	1.62	1.53	2.00	1.84	1.85
$k_{v2,B4}$	1.21	1.03	1.24	1.3	1.27	1.31
$k_{v2,C4}$	2.14	2.01	2.22	2.3	2.03	2.00
$k_{v2,D4}$	1.40	1.16	1.42	1.50	1.46	1.51
$k_{v2,E4}$	1.20	0.96	1.22	1.30	1.25	1.31

from 0% to 60%, the voltage unbalance rises. However, for higher penetration levels, k_{v2} does not change significantly. This phenomenon is illustrated more clearly in Table V. For example, at the LV busbar, the average value of k_{v2} increases until 60% penetration level, where $k_{v2,LV}$ = 0.3%. Above this penetration level, k_{v2} stabilizes around 0.3%. Regarding the remaining buses, the average value of k_{v2} follows an increasing trend with higher EV penetration levels across the system except for the end of feeder D (bus D4), where a reduction of the average value is recorded for penetration levels above 60%. Table VI shows that the peak values of k_{v2} follow a similar trend as the average values.

Overall, by comparing the effect of PVs and EVs on voltage unbalance, it can be inferred that while increasing the number of PVs installed causes a rise in voltage unbalance up to a certain penetration level (i.e. 60%), the penetration of EVs generally results in higher voltage unbalance with increasing penetration levels. This is due mostly to the high rating of the EVs (3 kW), and the fact that the EVs act as loads, therefore increasing the unbalance levels when they are connected to the system. On the other hand, PV ratings are generally smaller (with ratings provided in Section III) and they act as generators, thus contributing to supply the local loads as their penetration increases, and therefore resulting in a reduction of voltage unbalance.

C. Deployment of BESS for voltage unbalance mitigation

The proposed control strategy was tested for an operating condition with 60% PV and 20% EV penetration level. This scenario was chosen because it resulted in high voltage unbalance during certain times of the day. Various BESS locations were tested, specifically: LV, A2, A4, C2 and C4. These busbars are highlighted in Figure 4 with green squares. They were chosen based on two criteria: LV is the low voltage side of the transformer, and the highest unbalance originates from feeder A and feeder C.

The results are shown for the time between 14:00 h and 17:00 h to capture the effect of both PVs and EVs on voltage unbalance. Figure 7 presents the simulation results of k_{v2} for a summer day. For buses C4, D4, E4, the results are plotted without and with the BESSs placed at busbar LV in order to observe the impact of the BESS control on mitigating the unbalance. The graphs for buses LV, A4, B4 have been omitted for brevity. The superscript 'c' in k_{v2} denotes the voltage unbalance factor of the compensated system.

Table VII and Table VIII show the average and peak values of k_{v2} calculated over the 3-hour period, respectively. In the table, yellow highlights are used to indicate the minimum value for each busbar. Table VII shows that the BESS placement at busbar LV leads to the minimization of the voltage unbalance

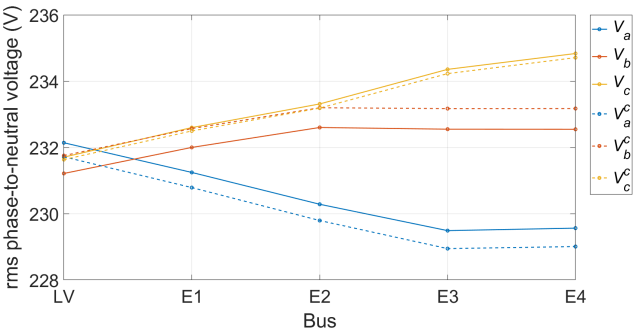

Fig. 8. rms phase-to-neutral voltage across feeder E for the compensated system (dashed line) and the uncompensated system (continuous line).

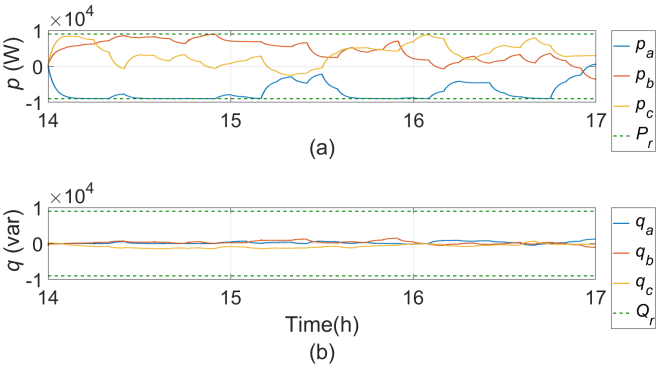

Fig. 9. (a) Active and (b) reactive power of the BESS inverters connected at busbar LV

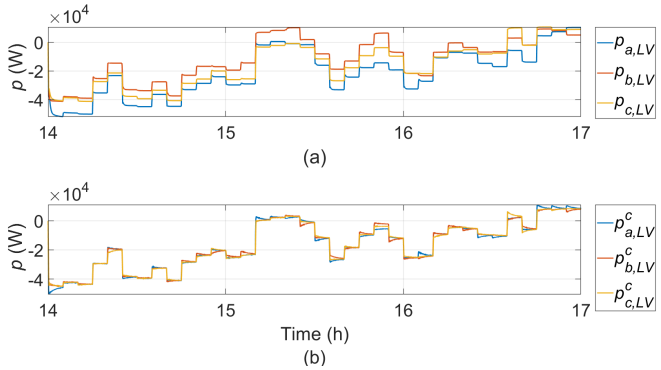

Fig. 10. Active power flows at busbar LV: (a) without BESSs (b) with BESSs connected.

factor at buses LV, B4, D4 and E4. This result means that in general, the more upstream the BESS is connected, the highest is its mitigating effect on voltage unbalance in the downstream buses. The maximum reduction of k_{v2} at bus A4 and bus C4 is achieved for BESS location in the middle of feeder A (bus A2) and in the end of feeder C (bus C4), respectively. This result can be explained by the high unbalance originated at these feeders, that require installation of BESS in close proximity to the loads. Table VIII shows similar results in terms of peak value. In particular, the peak unbalance at bus C4 is reduced below the standard limits. It is worth noticing that in this model the voltage source is considered symmetrical, while in the practice voltage unbalance levels may be higher thus making the proposed control more attractive to mitigate voltage unbalance locally.

Based on Figure 7, one can observe that the BESS control reduces the voltage unbalance factor throughout the simulation period, except a few time periods during which k_{v2} increases. For instance, igure 7(c) shows that with the BESS connected to the LV busbar, the unbalance levels at the end of feeder E (bus E4) rise between 15:00-15:20 h. These times coincide with high PV generation at phase-b and phase-c at bus E4 during this period, and more investigation was carried out to interpret this result.

More specifically, Figure 8 shows the rms voltage values recorded at 15:08 h across feeder E, for the case without compensation and for the case when the BESS units are installed at busbar LV. For the uncompensated system, phase-b voltage (V_b) and phase-c voltage (V_c) values (red and yellow continuous line) increase across the feeder due to the presence of PVs in these two phases. For the compensated system, the contribution of BESSs causes the three rms voltage values (dashed line) to converge at busbar LV ($V_a^c = V_b^c = V_c^c$), i.e. phase-a and phase-c voltage decrease, while phase-b voltage increases. This is the expected result from the proposed control system algorithm. As a result, in the compensated system, phase-a and phase-c voltages are translated downward, while phase-b voltages are translated upward across the system, thus resulting in an increased deviation between the voltages at bus E4 and as a result an increased voltage unbalance factor value. This result highlights the importance of monitoring the impact of the proposed strategy across the system to identify the best location.

Figure 9 shows the active and reactive power exchange of the BESS units installed at busbar LV for a time frame where high level of unbalance is observed. The active power of phase-a BESS inverter is negative throughout the simulation period, meaning that phase-a BESS unit charges, while phase–b and phase-c BESS units discharge throughout most of the simulation period to mitigate the unbalance. The amount of reactive power absorbed or injected by the BESS units is significantly lower than the active power, since the system unbalance is mostly due to active power unbalance. Figure 9 shows that there are time intervals during which phase-a BESS active power is saturated to the limit of 9 kVA. As a result of output saturation, the voltage unbalance is not fully eliminated at busbar LV, i.e. $k_{v2,LV} = 0.05$ %, as shown in Table VII. Voltage unbalance could be further reduced if BESSs of larger size were installed at this location. However, this may not be necessary as voltage unbalance levels are mitigated to acceptable values.

For BESS located at other busbars, the power exchange with the system is significantly lower and no saturation is observed. For example, it was found that the maximum power exchange between the BESS and the grid is 3 kW and 4 kW for BESS placement at feeder A and C, respectively. These results are in agreement with the ones obtained in [31], where it was shown that the BESS power exchange is reduced when BESSs are placed downstream due to lower load demand at these locations. As a result, a BESS with lower rating may be installed at feeders A and C without compromising

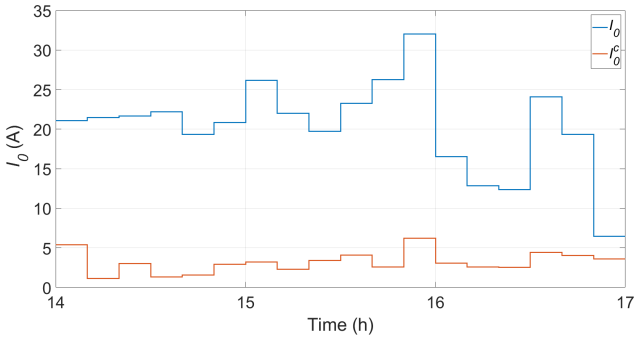

Fig. 11. Zero-sequence current component at busbar LV without (blue) and with (orange) compensation.

effectiveness of unbalance compensation. In this work, the same battery size was considered at all locations for simplicity, but in a practical application the battery rating will be chosen as a compromise between performance, cost, ancillary services provided and their remuneration [31].

Figure 10(a)-(b) show the active power flows at busbar LV without ($p_{i,LV}$) and with ($p^c_{i,LV}$) the proposed control strategy for BESS units connected at busbar LV, respectively. The compensating action performed by the three BESS units results in balanced power flows at the substation, therefore more effective utilization of the distribution line and transformer capacity can be achieved. Similar results were obtained for the reactive power profiles, which are omitted here for brevity.

The 10-min aggregated values of the zero-sequence current component of the transformer are plotted in Figure 11: these results show that the proposed control strategy can alleviate the current flowing in the neutral conductor.

Based on the positive results obtained in the simulation environment, the next step consisted in experimental validation that will be described in the next section.

V. Experimental Results

To validate the control strategy experimentally, Hardware-In-The-Loop (HIL) tests were carried out. Figure 12 shows the laboratory setup: an OP5600 real-time simulator was used to run the grid, load and inverter models in real time. The simulation models were modified using RT-LAB (OPAL-RT's software platform) and they were loaded in the simulator. The communication between the computer and the OPAL-RT was established via an Ethernet cable. The PELab-3PHHPLC is a power electronics development system consisting of a configurable inverter and an embedded controller based on ARM Cortex M7/M4 dual-core microcontroller, which is programmed with the use of Keil software. PELab exchanges analogue and digital signals with OPAL-RT by means of DB37 connector cables.

In this work, the control algorithm was implemented in OPAL-RT, with the microcontroller being responsible for generating the PWM signals. More specifically, as shown in Figure 13, the closed-loop controller calculates and sends the reference voltage $v_{a,ref}$ to the microcontroller, which generates the switching signals (s_1, s_2) for the single-phase inverter connected at phase-a. In this paper only single-phase inverter operation is carried out due to equipment limitations.

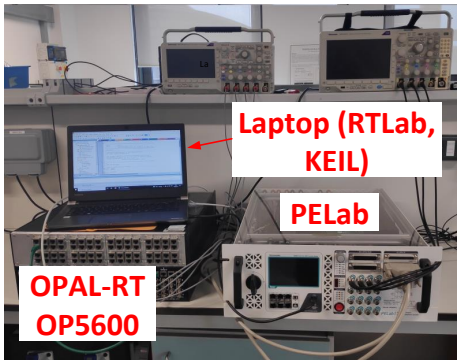

Fig. 12. Laboratory setup including the PELab-3PHHPLC and OPAL-RT simulator managed by the RT-LAB and Keil software respectively.

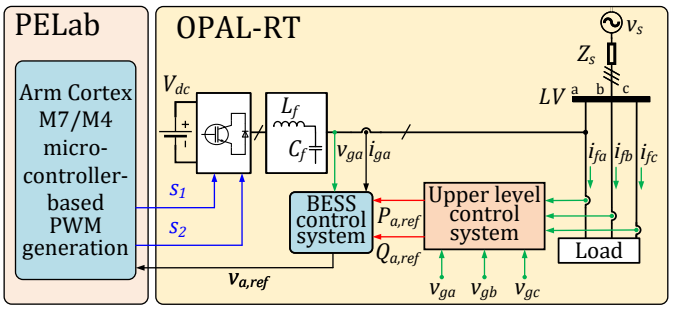

Fig. 13. Real time simulation model and overview of the control scheme and signals.

TABLE IX
Experimental parameters.

Parameters	Values
rms grid voltage	$V_s = 230$ V
Source impedance	$\boldsymbol{Z_s}$ = 0.0716 + j0.0504 Ω
Switching and sampling frequency	$f_{sw} = f_s = 5$ kHz
PI power controller	$k_{pp} = 0.1$, $k_{pq} = 0.1$ $k_{ip} = 10$ s^{-1}, $k_{iq} = 10$ s^{-1}
PR current controller	$k_{pi} = 5$ Ω , $k_{ii} = 70$ Ωs^{-1}
Three-phase Load 1 (L1)	$P_{L1i} = 100$ kW, $Q_{L1i} = 5$ kvar, i = a,b,c
Three-phase Load 2 (L2)	$P_{L2a} = 15$ kW, $Q_{L2a} = 2$ kvar, $P_{L2b} = 6$ kW, $Q_{L2b} = 1$ kvar, $P_{L2c} = 2$ kW, $Q_{L2c} = 0.5$ kvar
Single-phase Load 3 (L3)	$P_{L3a} = 5$ kW, $Q_{L3a} = 1$ kvar

However, it is worth emphasizing that this approach is still valid to test the proposed strategy. As Figure 13 shows, phase-a voltage and current (v_{ga}, i_{ga}) are measured at the inverter terminal to be used in the BESS control system, while phase-a voltage and the three phase feeder currents' readings (v_{ga} and i_{fi} for i = a, b, c) are needed for the upper level control system to calculate phase-a reference power, as given in (1).

The circuit modelled in OPAL-RT consists of three symmetrical voltage sources connected to an unbalanced load via impedances. The BESS was modelled using a constant DC voltage source. The PR controller gains were modified compared to the values used in the offline simulations to obtain a stable response. Additionally, the switching frequency was reduced to 5 kHz to satisfy OPAL-RT platform requirements [32]. Table IX summarizes the experimental parameters.

To validate the developed control strategy experimentally,

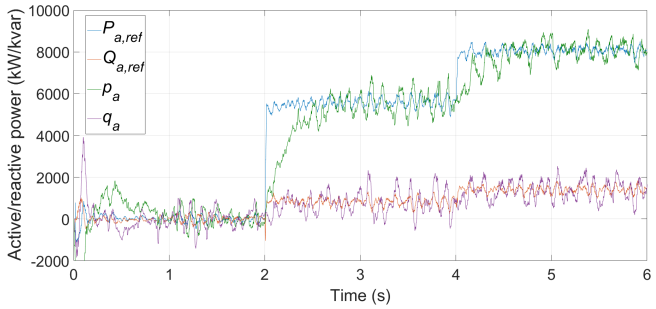

Fig. 14. Active and reactive power injected by phase-a inverter.

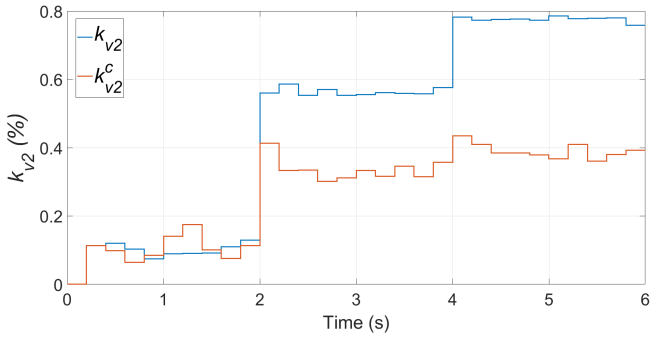

Fig. 15. Voltage unbalance factor at busbar LV, without (blue) and with (orange) compensation.

a single BESS unit connected at phase-a was controlled to mitigate the unbalance caused by three-phase and single-phase loads. Initially, a balanced load L1 was connected to the system. At $t = 2$ s, an unbalanced load L2 was added in parallel, and at $t^{'} = 4$ s the unbalance at phase-a was further increased by adding the load L3 at the same phase. The loads active and reactive powers are provided in Table IX.

The active and reactive power injections from phase-a inverter are shown in Figure 14. Figure 15 shows the voltage unbalance factor profiles without BESS (k_{v2}) and with BESS connected (k^c_{v2}) aggregated over 200 ms for a simulation period of 6 s. The aggregation window in this case is different from the one used in simulation, as shorter times are monitored. However, both aggregation windows are used in practical applications, as described in IEC 61000-2-2 [28]. Between t = 0 s and t = 2 s, the unbalance is close to zero since the load is balanced. At t = 2 s, the unbalanced load is introduced and k_{v2} = 0.57% for the uncompensated system. For the compensated system, the BESS inverter injects active and reactive power equal to p_a = 5.5 kW and q_a = 0.8 kvar. As a result, the phase-a power flow through busbar LV is reduced and a more balanced power flow is obtained, leading to a lower voltage unbalance factor value, i.e. k^c_{v2} = 0.33%. At $t^{'}$ = 4 s, k_{v2} increases to 0.77% due to the additional load connected at phase-a. Therefore, the controller responds by further increasing the injection of active and reactive power to p_a = 8 kW and q_a = 1.4 kvar, respectively.

This case study demonstrates that the developed control strategy can effectively mitigate voltage unbalance for the case when an individual BESS is connected. Further reduction or full unbalance mitigation will require providing zero- and negative-sequence load current component at phase-b and phase-c by the other two inverters.

VI. Conclusion

In this paper, a novel control strategy that uses three single-phase BESS inverters to provide voltage unbalance mitigation as ancillary service has been presented. The BESS units are managed by an upper level control system that calculates the reference power signals based on inverter voltage and feeder current measurements. The local control system is then responsible to generate the switching pulses for the inverters. It was shown that under the presented control strategy, the BESS inverters can exchange active and reactive power appropriately at each phase thus mitigating voltage unbalance.

Simulations were realized in a typical UK distribution network consisting of realistic profiles of residential demand, PVs and EVs. Initially, the effect of varying penetration of PVs and EVs on voltage unbalance was examined, showing that these two technologies may have a different impact on the system unbalance.

The effectiveness of the unbalance compensation scheme was demonstrated for a simulation scenario in which both PVs and EVs were connected to the distribution system. The results have shown that the BESS units have the capability to provide an overall reduction in the unbalance levels, decrease the neutral current and equalize the power flows at the substation, thereby enabling a more effective utilization of the feeder and transformer capacity.

Finally, the control strategy was validated experimentally by performing HIL tests. In this case, a single-phase inverter was considered due to equipment limitation. The experiment shows that the BESS unit was able to compensate voltage unbalance by injecting both active and reactive power, demonstrating the potential of the developed control scheme to provide a substantial reduction of voltage unbalance even in the case when only a unit is available to provide such ancillary service.

This work allowed identifying several future research topics:

- Probabilistic simulations will be carried out to reinforce the conclusions of this work, that is currently based on a deterministic approach.
- The integration of the proposed strategy with other control features will be addressed, both in stand-alone batteries and in other devices, including EVs.
- The provision of unbalance compensation adds additional rating requirements, and therefore adequate remuneration should be associated with this service. At the same time, this solution may be attractive for the DNOs as it allows mitigating voltage unbalance without the installation of additional equipment. Economic considerations will be the subject of future work.

VII. Acknowledgement

The authors gratefully acknowledge EPSRC (Engineering and Physical Sciences Research Council) grant number EP/T013206/2.

References

[1] I. Mexis and G. Todeschini, "Battery Energy Storage Systems in the United Kingdom: A Review of Current State-of-the-Art and Future Applications," Energies, vol. 13, no. 14, 2020.

[2] L. Hadjidemetriou, A. Charalambous, and E. Kyriakides, "Control Scheme for Phase Balancing of Low-Voltage Distribution Grids," in 2019 International Conference on Smart Energy Systems and Technologies (SEST), 2019, pp. 1–6.
[3] K. Ma, L. Fang, and W. Kong, "Review of Distribution Network Phase Unbalance: Scale, Causes, Consequences, Solutions, and Future Research Directions," CSEE Journal of Power and Energy Systems, vol. 6, no. 3, pp. 479–488, 2020.
[4] J. M. Guerrero, P. C. Loh, T.-L. Lee, and M. Chandorkar, "Advanced Control Architectures for Intelligent Microgrids—Part II: Power Quality, Energy Storage, and AC/DC Microgrids," IEEE Transactions on Industrial Electronics, vol. 60, no. 4, pp. 1263–1270, 2013.
[5] M. Castilla, J. Miret, A. Camacho, J. Matas, and L. García de Vicuña, "Voltage Support Control Strategies for Static Synchronous Compensators Under Unbalanced Voltage Sags," IEEE Transactions on Industrial Electronics, vol. 61, no. 2, pp. 808–820, 2014.
[6] F. Nejabatkhah, Y. Li, and B. Wu, "Control Strategies of Three-phase Distributed Generation Inverters for Grid Unbalanced Voltage Compensation," in 2015 IEEE Energy Conversion Congress and Exposition (ECCE), 2015, pp. 6467–6474.
[7] F. Nejabatkhah and Y. W. Li, "Flexible Unbalanced Compensation of Three-Phase Distribution System Using Single-Phase Distributed Generation Inverters," IEEE Trans. on Smart Grid, vol. 10, no. 2, pp. 1845–1857, March 2019.
[8] F. Nejabatkhah, Y. W. Li, and H. Tian, "Power Quality Control of Smart Hybrid AC/DC Microgrids: An Overview," IEEE Access, vol. 7, pp. 52 295–52 318, 2019.
[9] R. Caldon, M. Coppo, and R. Turri, "Distributed Voltage Control Strategy for LV Networks With Inverter- interfaced Generators," Electric Power Systems Research, vol. 107, pp. 85 – 92, 2014.
[10] M. Yao, I. A. Hiskens, and J. L. Mathieu, "Mitigating Voltage Unbalance Using Distributed Solar Photovoltaic Inverters," IEEE Transactions on Power Systems, vol. 36, no. 3, pp. 2642–2651, 2021.
[11] M. J. E. Alam, K. M. Muttaqi, and D. Sutanto, "Community Energy Storage for Neutral Voltage Rise Mitigation in Four-Wire Multigrounded LV Feeders With Unbalanced Solar PV Allocation," IEEE Transactions on Smart Grid, vol. 6, no. 6, pp. 2845–2855, 2015.
[12] J. Fernandez, S. Bacha, D. Riu, H. Turker, and M. Paupert, "Current Unbalance Reduction in Three-phase Systems Using Single Phase PHEV Chargers," in 2013 IEEE International Conference on Industrial Technology (ICIT), Feb 2013, pp. 1940–1945.
[13] K. H. Chua, Y. S. Lim, P. Taylor, S. Morris, and J. Wong, "Energy Storage System for Mitigating Voltage Unbalance on Low-Voltage Networks With Photovoltaic Systems," IEEE Transactions on Power Delivery, vol. 27, no. 4, pp. 1783–1790, 2012.
[14] W. Pinthurat and B. Hredzak, "Distributed Control Strategy of Single-Phase Battery Systems for Compensation of Unbalanced Active Powers in a Three-Phase Four-Wire Microgrid," Energies, vol. 14, no. 24, 2021.
[15] M. J. E. Alam, K. M. Muttaqi, and D. Sutanto, "Alleviation of Neutral-to-Ground Potential Rise Under Unbalanced Allocation of Rooftop PV Using Distributed Energy Storage," IEEE Transactions on Sustainable Energy, vol. 6, no. 3, pp. 889–898, 2015.
[16] P. Tenti, D. Trombetti, E. Tedeschi, and P. Mattavelli, "Compensation of Load Unbalance, Reactive Power and Harmonic Distortion by Cooperative Operation of Distributed Compensators," in 2009 13th European Conference on Power Electronics and Applications, 2009, pp. 1–10.
[17] I. Mexis and G. Todeschini, "Voltage Unbalance Mitigation by Novel Control of BESS Single–phase Inverters," in 2020 IEEE PES Innovative Smart Grid Technologies Europe (ISGT-Europe), 2020, pp. 146–150.
[18] M. Ciobotaru, R. Teodorescu, and F. Blaabjerg, "A New Single-phase PLL Structure Based on Second Order Generalized Integrator," in 2006 37th IEEE Power Electronics Specialists Conference, June 2006, pp. 1–6.
[19] S. Golestan, M. Monfared, F. D. Freijedo, and J. M. Guerrero, "Dynamics Assessment of Advanced Single-Phase PLL Structures," IEEE Trans. on Industrial Electronics, vol. 60, no. 6, pp. 2167–2177, 2013.
[20] C. Zhang, X. Wang, F. Blaabjerg, W. Wang, and C. Liu, "The Influence of Phase-Locked Loop on the Stability of Single-phase Grid-connected Inverter," in 2015 IEEE Energy Conversion Congress and Exposition (ECCE), 2015, pp. 4737–4744.
[21] A. Nagliero, R. A. Mastromauro, M. Liserre, and A. Dell'Aquila, "Monitoring and Synchronization Techniques for Single-phase PV Systems," in SPEEDAM 2010, June 2010, pp. 1404–1409.
[22] Y. Yang, F. Blaabjerg, and Z. Zou, "Benchmarking of Grid Fault Modes in Single-Phase Grid-Connected Photovoltaic Systems," IEEE Transactions on Industry Applications, vol. 49, no. 5, pp. 2167–2176, 2013.
[23] R. Teodorescu, F. Blaabjerg, M. Liserre, and P. C. Loh, "Proportional-resonant Controllers and Filters for Grid-connected Voltage-source Converters," IEE Proceedings-El. P. Ap., vol. 153, no. 5, pp. 750–762, 2006.
[24] C. Yanarates and Z. Zhou, "Symmetrical Pole Placement Method-Based Unity Proportional Gain Resonant and Gain Scheduled Proportional (PR-P) Controller With Harmonic Compensator for Single Phase Grid-Connected PV Inverters," IEEE Access, vol. 9, pp. 93 165–93 181, 2021.
[25] I. Hernando-Gil, H. Shi, F. Li, S. Djokic, and M. Lehtonen, "Evaluation of Fault Levels and Power Supply Network Impedances in 230/400 V 50 Hz Generic Distribution Systems," IEEE Transactions on Power Delivery, vol. 32, no. 2, pp. 768–777, 2017.
[26] A. Navarro-Espinosa and L. F. Ochoa, "Probabilistic Impact Assessment of Low Carbon Technologies in LV Distribution Systems," IEEE Transactions on Power Systems, vol. 31, no. 3, pp. 2192–2203, 2016.
[27] Electricity North West, "Low Voltage Network Solutions (LVNS) - Project literature," https://www.enwl.co.uk/lvns, [Online; accessed 14-April-2022].
[28] IEC-Internat. Electrot. Commis. and others, "IEC 61000-2-2," 2002.
[29] "IEEE Recommended Practice for Monitoring Electric Power Quality," IEEE Std 1159-2009 (Revision of IEEE Std 1159-1995), pp. 1–94, 2009.
[30] IEC-Internat. Electrot. Commis. and others, "IEC 61000-4-30," 2015.
[31] I. Mexis, G. Todeschini, F. Möller, and J. Meyer, "Mitigation of Voltage Unbalance in Rural Low Voltage Networks Using Single-phase BESS Inverters," in CIRED 2021 - The 26th International Conference and Exhibition on Electricity Distribution, vol. 2021, 2021, pp. 789–794.
[32] OPAL-RT, "RT-LAB Software home page," https://www.opal-rt.com/software-rt-lab-2-2/, [Online; accessed 13-April-2022].

Ioannis Mexis received the M.Eng. degree in Electrical and Computer Engineering from Aristotle University of Thessaloniki, Thessaloniki, Greece, in 2014 and the M.Sc. degree in Power Electronics and Drives from Aalborg University, Aalborg, Denmark in 2018. He is currently pursuing the Ph.D. degree with the Electrical and Electronic Engineering Department in Swansea University, Swansea, UK. His research interests include design of ancillary services for battery energy storage systems, control of power converters and their applications in power systems.

Grazia Todeschini (M'10–SM'14) is a Reader at King's College London and Honorary Senior Lecturer at Swansea University. She received her PhD in 2010 from the Worcester Polytechnic institute and then worked for EnerNex in Knoxville, TN and for General Electric in Philadelphia, PA. Her research interest includes the modeling and simulation of power system for power quality assessment, the study of power quality disturbances and development of ancillary services for distributed resources. Dr. Todeschini is IEEE Senior Member, IET Member and Fellow of the Higher Education Academy.

Zhongfu Zhou received the Ph.D. degree from the University of Sussex, Brighton, U.K., in 2004. He joined the College of Engineering, Swansea University, in 2004, as a Research Officer, and promoted as a Lecturer in power electronics, in July 2016. His research interests include active rectifier, active power filter, and power electronics applications for renewable energy systems and automotive. Since 2010, he has been a member of the International Electrotechnical Commission (IEC), where he has advised on the international standard (IEC TS 62600- 30) on electrical power quality requirements for wave, tidal, and other water current energy converters.